Near-Field Effects on Micrometer Accurate Ranging With Ultra-Wideband mmWave Radar

Lukas Piotrowsky, *Student Member, IEEE*, Jan Barowski, *Senior Member, IEEE*, and Nils Pohl, *Senior Member, IEEE*

***Abstract*—We investigated near-field effects on free-space ranging with ultra-wideband millimeter-wave (mmWave) radar. In this application, one often assumes far-field conditions. However, with increasing requirements of accuracy, far-field assumptions are not satisfying. The radar measurements are affected by phase variations, leading to erroneous distance estimates. To simulate and approximate these effects, we propose computational methods by means of physical optics. They were validated using a state-of-the-art frequency-modulated continuous-wave radar sensor. Sophisticated experiments show good agreement; thus, in practice, the methods can be used to correct distance estimates to achieve micron accuracy without extensive calibration in advance.**

***Index Terms*—Distance measurement, millimeter-wave (mmWave) radar, near-field effects, phase center, radar theory, scattering center.**

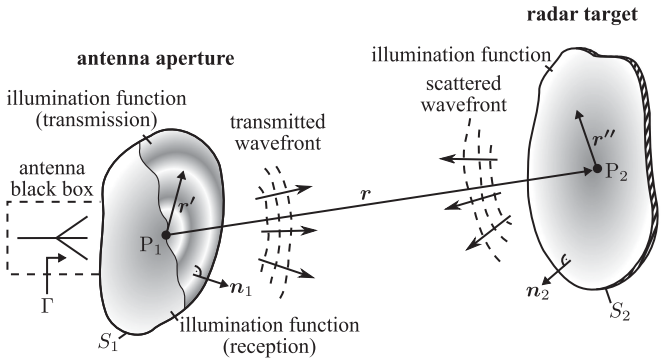

Fig. 1. Geometry of the investigated problem.

I. Introduction

RANGE measurement (ranging) with monostatic radar refers to measuring the distance between the reference points of the antenna and the radar target. One often assumes far-field conditions, i.e., point sources of radiation, point scatterer, and planar wavefronts; then the reference points are described by the concept of antenna phase center [1]–[7] and the scattering center of the radar target [8]–[10].

However, far-field assumptions are not satisfying if the application requires very high accuracy [11]–[23], e.g., for machine calibration as an alternative to optical metrology [12]. Antenna aperture and target cross section are not point-shaped, and generally, they are inhomogeneously illuminated in amplitude and phase. Therefore, the radiated and the scattered wavefronts are curved. More precisely, only with increasing distance of observation, the equiphase surfaces of curved wavefronts become concentric spheres originating at the antenna phase center and the target scattering center, respectively.

This leads us to the definition of the near-field variation of reference points as the deviation of the actual position of reference points in radar measurements—which are not related to any physical point in space—from the far-field centers of the antenna and the target. Hence, phase variations occur in real-world radar measurements as a function of frequency, orientation, and distance.

Since ultra-wideband millimeter-wave (mmWave) radar offers a very high range resolution of a few millimeters, it allows micrometer accurate distance measurements [11]–[13], [17]. In [12], we identified near-field variation of reference points[1] as a major source of systematic errors on linear position measuring. This measurement error is of increasing importance when the mmWave sensor becomes more technologically advanced in terms of bandwidth, frequency stability, phase noise, and linearity. The key contribution of this letter is, for the first time to the best of our knowledge, an in-depth investigation of this small but significant effect on highly accurate ranging.

II. Theory of Near-Field Phase Variations

Fig. 1 depicts the geometry of the investigated problem, where S_1 and S_2 are planar surfaces bounding the antenna aperture and the target cross section, respectively. The surfaces are characterized by their centers P_1 and P_2, their normal vectors $\boldsymbol{n}_1$ and $\boldsymbol{n}_2$, and their relative position $\boldsymbol{r}$. Furthermore, $\boldsymbol{r'}$ and $\boldsymbol{r''}$ are vectors in S_1 and S_2, respectively. Since the range resolution of ultra-wideband hardware is very high, the investigation is limited to the line-of-sight path. Multiple reflections are therefore neglected.

According to Schelkunoff's equivalence principle [24], sources of electromagnetic (EM) radiation, e.g., transmitting antennas, inside a closed surface can be expressed by means of a

Manuscript received January 14, 2022; revised February 11, 2022; accepted February 14, 2022. Date of publication February 18, 2022; date of current version May 5, 2022. This work was supported in part by the German Research Foundation (DFG) under Project-ID 287022738 – TRR 196; and in part by the Federal Ministry of Education and Research of Germany (BMBF) under Grant 16ME0179. *(Corresponding author: Lukas Piotrowsky.)*

Lukas Piotrowsky and Nils Pohl are with the Institute of Integrated Systems, Ruhr University Bochum, 44801 Bochum, Germany (e-mail: lukas.piotrowsky@rub.de; nils.pohl@rub.de).

Jan Barowski is with the Institute of Microwave Systems, Ruhr University Bochum, 44801 Bochum, Germany (e-mail: jan.barowski@rub.de).

Digital Object Identifier 10.1109/LAWP.2022.3152558

[1]Incorrectly referred to as phase-center variations.

fictitious magnetic surface current to produce the same electric and magnetic field outside the closed surface. As a transmitting aperture antenna primarily radiates from its physical aperture, the equivalence principle can be applied to a surface bounded by that aperture. Let $\underline{\boldsymbol{E}}^{+}(\boldsymbol{r'})$ be the complex amplitude of the electric field of the transmitted monochromatic wave on the antenna aperture, simulated by full-wave EM simulation. Then, the equivalent magnetic surface current density is

$$\underline{\boldsymbol{M}}_S^{\mathrm{ant}}(\boldsymbol{r'}) = 2\underline{\boldsymbol{E}}^{+}(\boldsymbol{r'}) \times \boldsymbol{n}_1. \tag{1}$$

Thus, the transmitting antenna is a black box fully described by the magnetic surface current density on its aperture.

The illuminated radar target is also substituted by a distribution of equivalent current densities, taking into account the fields radiated by the equivalent magnetic surface current of the antenna. The planar radar target is assumed to be perfectly conducting, and it is large compared to the wavelength. Consequently, edge effects are negligible, the tangential component of the incident electric field vanishes, and there is no cross polarization. Assuming the radar target is at least several wavelengths away from the antenna, then the equivalent electric and magnetic current densities on the target surface are given by the principle of physical optics [25] as

$$\underline{\boldsymbol{J}}_S^{\mathrm{tar}}(\boldsymbol{r''}) = \frac{2\mathrm{j}k\boldsymbol{n}_2}{Z_0} \times \iint_{S_1} \boldsymbol{e_R} \times \left[\boldsymbol{e_R} \times \underline{\boldsymbol{M}}_S^{\mathrm{ant}}(\boldsymbol{r'})\right] \underline{G}(R)\,\mathrm{d}\boldsymbol{S} \tag{2}$$

and

$$\underline{\boldsymbol{M}}_S^{\mathrm{tar}}(\boldsymbol{r''}) = \boldsymbol{0}, \tag{3}$$

respectively. Here, k is the wavenumber, Z_0 is the impedance of free space, $\boldsymbol{R}$ substitutes

$$\boldsymbol{R} = -\boldsymbol{r'} + \boldsymbol{r} + \boldsymbol{r''}, \tag{4}$$

$\boldsymbol{e_R}$ is the unit vector in the direction of $\boldsymbol{R}$, and $\underline{G}(R)$ is Green's function

$$\underline{G}(R) = \frac{\exp(-\mathrm{j}kR)}{4\pi R}. \tag{5}$$

The scattered electric field incident on the antenna aperture is then given by

$$\underline{\boldsymbol{E}}^{-}(\boldsymbol{r'}) = \mathrm{j}kZ_0 \iint_{S_2} \boldsymbol{e_R} \times \left[\boldsymbol{e_R} \times \underline{\boldsymbol{J}}_S^{\mathrm{tar}}(\boldsymbol{r''})\right] \underline{G}(R)\,\mathrm{d}\boldsymbol{S}. \tag{6}$$

The reflecting system is described by a reflection coefficient depending on the distribution of the electric field of the transmitted and received wavefronts, i.e., on the aperture illumination functions. Provided that the antenna's feed line is in single-mode operation, a linear relationship is assumed between the waves on the feed line and the electric field components on the aperture [26]. Only components of $\underline{\boldsymbol{E}}^{-}(\boldsymbol{r'})$ that are matched to the reception properties of the antenna contribute to the outgoing wave on the feed line. As reciprocal antennas have the same transmission and reception properties, one can assume a reflection coefficient

$$\Gamma = -\frac{\iint_{S_1} \underline{\boldsymbol{E}}^{+}(\boldsymbol{r'}) \cdot \underline{\boldsymbol{E}}^{-}(\boldsymbol{r'})\,\mathrm{d}\boldsymbol{S}}{\iint_{S_1} \underline{\boldsymbol{E}}^{+}(\boldsymbol{r'}) \cdot \underline{\boldsymbol{E}}^{+}(\boldsymbol{r'})\,\mathrm{d}\boldsymbol{S}} \tag{7}$$

which is related to the aperture plane neglecting antenna mismatch. Equation (7) was described similarly by the authors in [27] and [28]. Note that the dot product of complex vectors $\underline{\boldsymbol{a}} \cdot \underline{\boldsymbol{b}}$ is defined as $\underline{\boldsymbol{a}}^{\mathrm{H}}\underline{\boldsymbol{b}}$, where $\underline{\boldsymbol{a}}^{\mathrm{H}}$ denotes the Hermitian transpose of $\underline{\boldsymbol{a}}$.

The near-field variation of reference points is related to the reflection coefficient under far-field conditions

$$\Gamma_{\mathrm{ref}} = -\frac{G_{\mathrm{ant}}\lambda}{|\boldsymbol{r}|^2}\sqrt{\frac{\sigma}{(4\pi)^3}}\exp(-\mathrm{j}k2|\boldsymbol{r}|) \tag{8}$$

where the amplitude term is based on the radar range equation, and the phase term applies to a reflected plane wave propagating from P_1 to P_2 and vice versa. Here, G_{ant} is the antenna gain, λ is the wavelength, and σ is the target's radar cross section.

Finally, the resulting phase variation due to near-field effects is

$$\phi_{\mathrm{var}} = \arg\left\{\frac{\Gamma}{\Gamma_{\mathrm{ref}}}\right\}. \tag{9}$$

In general, the amplitude of the reflected signal is also affected, which is expressed as a gain factor

$$\alpha = \left|\frac{\Gamma}{\Gamma_{\mathrm{ref}}}\right|. \tag{10}$$

However, as the effect on amplitude is quasi-independent of frequency, it does not significantly bias the radar measurement. Thus, it is neglected and not subject to further investigation.

Readers interested in microwave diffraction, scattering matrix description of waveguide-space transducers, and reciprocity relations may refer to the work in [26].

III. Effects on Time-Domain Estimates

Apart from pure continuous-wave (CW) radar, the working principle of radar is to measure the band-limited impulse response of the two-way radar path as given by

$$\underline{h}(t) = A \cdot \underline{g}(t-\tau) \cdot \exp(-\mathrm{j}\omega_{\mathrm{c}}\tau) \tag{11}$$

for a single radar target. Here, A^{-1} is the attenuation, $\underline{g}(t)$ is the pulse shape, τ is the time of flight, and ω_{c} is the center angular frequency. Using frequency-modulated short-range radar, τ can be obtained with standard-resolution algorithms in time domain either by measuring the pulse position at the maximum in $|\underline{h}(t)|$ or by measuring the pulse phase by utilizing the phase factor $\exp(-\mathrm{j}\omega_{\mathrm{c}}\tau)$, which is beneficial, as discussed in [11]–[13], [16], [19], and [29].

Starting with a column vector

$$\boldsymbol{y} = [\phi_{\mathrm{var}}^{\omega_1} \quad \phi_{\mathrm{var}}^{\omega_2} \quad \dots \quad \phi_{\mathrm{var}}^{\omega_N}]^{\mathrm{T}} \tag{12}$$

of numerically computed phase variations $\phi_{\mathrm{var}}^{\omega_n}$ [see (9)] at N equally spaced angular frequencies ω_n, covering the bandwidth of the investigated radar pulse, then the variation of pulse position $\Delta\tau$ and the variation of pulse phase $\Delta\phi$ are conveniently computed via a linear least-squares method in frequency domain $\underline{H}(\mathrm{j}\omega) = \mathcal{F}\{\underline{h}(t)\}$ as

$$[\Delta\phi \quad \Delta\tau]^{\mathrm{T}} = (\mathbf{A}^{\mathrm{T}}\mathbf{A})^{-1}\mathbf{A}^{\mathrm{T}}\boldsymbol{y} \tag{13}$$

where

$$\mathbf{A} = \begin{bmatrix} 1 & 1 & \dots & 1 \\ \omega_c - \omega_1 & \omega_c - \omega_2 & \dots & \omega_c - \omega_N \end{bmatrix}^{\mathrm{T}} \tag{14}$$

is an N by two matrix, containing the respective frequency values. Finally, the simulated distance variations of the pulse position and pulse phase measurement are

$$\Delta r_\tau = \Delta\tau \frac{c}{2} \quad \text{and} \quad \Delta r_\phi = -\Delta\phi \frac{c}{2\omega_c}, \tag{15}$$

respectively. Here, c denotes the speed of light.

IV. Approximate Closed-Form Expression

For the matter of convenience, it is useful to have a closed-form expression for rapid computation of the approximate distance variation due to near-field effects. We examine the case of a planar circularly symmetric antenna aperture and a planar circularly symmetric radar target. Both are parallel to each other, and they lie on a line through their centers, which corresponds to a perfectly aligned target in the antenna boresight. The only geometric degrees of freedom left are the diameters and distance.

The investigated problem is divided into four subproblems: transmitted wave of the antenna, incident wave on the target, scattered wave at the target, and incident wave on the antenna. Scalar approximations were made; thus, polarization is neglected. The illumination functions of the transmitting antenna and the scattering radar target are assumed to be uniform in amplitude and phase. Furthermore, incident wavefronts are assumed to be spherical and of constant amplitude. Then, the respective phase variation for each of the cases mentioned earlier is expressed equivalently as

$$\phi'_{\mathrm{var}}(r) = \arg\left\{ \int_0^{D/2} r' \frac{\exp\left[-\mathrm{j}k\left(\sqrt{r^2 + r'^2} - r\right)\right]}{\sqrt{r^2 + r'^2}} \,\mathrm{d}r' \right\} \tag{16}$$

where r refers to the distance to the source of radiation or the distance to the observation point, and D is the diameter of the respective cross section. After applying Fresnel approximation, i.e., a first-order Taylor series expansion of the amplitude term and a second-order Taylor series expansion of the phase term, (16) is reduced to

$$\phi'_{\mathrm{var}}(r) = \arg\left\{ \mathrm{j}\left[\exp\left(-\frac{jkD^2}{8r} \right) - 1 \right] \right\} = -\frac{D^2}{16r}k. \tag{17}$$

Consequently, the total phase variation of the entire two-way radar path is

$$\phi_{\mathrm{var}}(r) = -2\frac{D_1^2}{16r}k - 2\frac{D_2^2}{16r}k \tag{18}$$

where D_1 and D_2 are the diameter of the antenna aperture and the diameter of the target, respectively. As (18) is of linear phase, we found a frequency-independent approximate closed-form expression of the distance variation due to near-field effects as

$$\Delta r(r) = \frac{D_1^2 + D_2^2}{16r}. \tag{19}$$

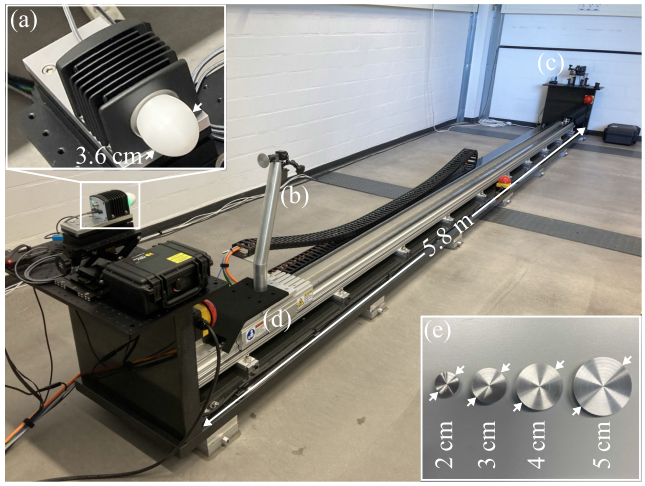

Fig. 2. Photograph of the experimental setup and its components: (a) radar sensor, (b) radar target and optical retro-reflector, (c) laser measurement system, (d) linear carriage, and (e) variety of radar targets used.

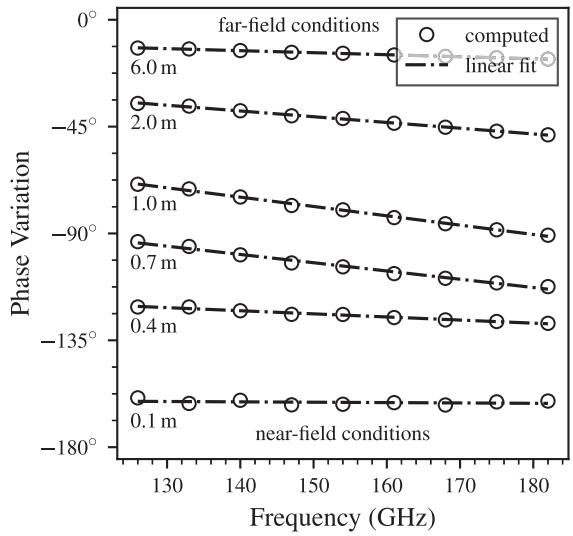

Fig. 3. Computed phase variations for the radar target with 5 cm of diameter at various distances from 0.1 to 6 m.

V. Simulations and Experiments

We conducted a series of simulations and experiments to validate the proposed theory. As a radar platform, we used the prototype of a state-of-the-art ultra-wide D-band sensor [30] in frequency-modulated continous-wave (FMCW) technology. The parameters of the radar are summarized in Table I. Fig. 2 shows a photograph of the experimental setup. We used four disc-shaped radar targets with diameters of 2, 3, 4, and 5 cm. The respective radar target was mounted on the carriage of a motorized linear guide with roughly 5 m of travel range. The random measurement error was within ± 20 nm to ± 4 μm, and it was further improved by averaging 100 consecutive readings. The position was referenced to a laser measurement system based on a Michelson interferometer, which has an accuracy of better than 0.4 μm/m. The antenna and the target were aligned such that the target travels along the antenna boresight to measure

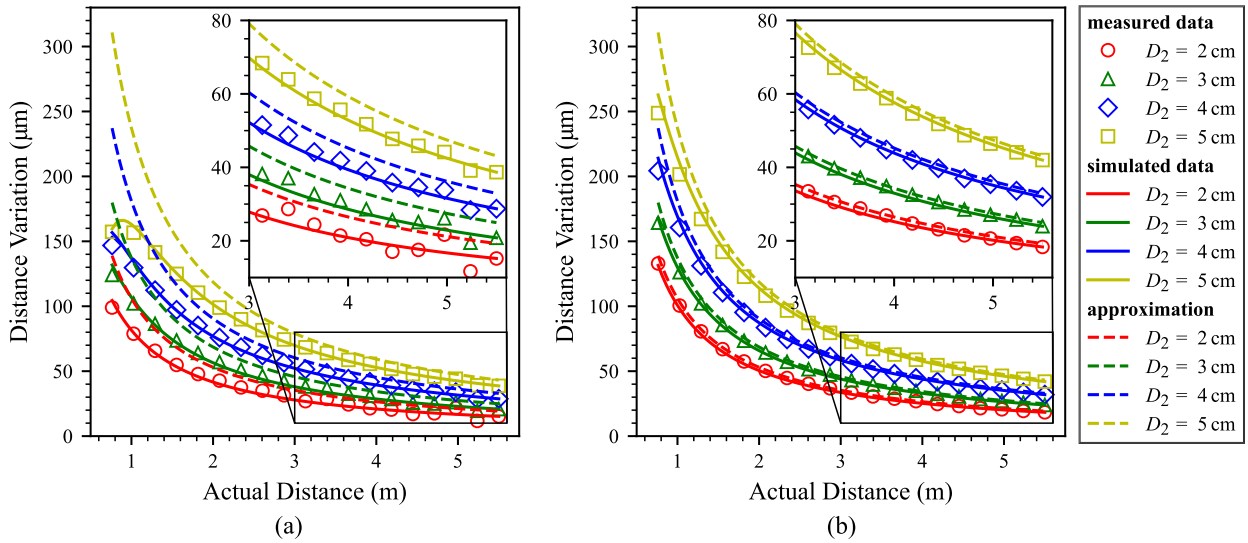

Fig. 4. Results of the measurements, the numerical simulations (see Sections II and III), and the approximate closed-form expression (19). Depicting the distance variations with respect to the actual distance for the radar targets of different sizes. Comparison of both principles of time-domain estimation: (a) pulse position measurement and (b) pulse phase measurement.

TABLE I
PARAMETERS OF THE RADAR SENSOR

Parameter	Value
Manufacturer (model)	2π-Labs (2πSENSE) [30]
Type	PLL stabilized D-band FMCW radar
Center frequency	154 GHz
Bandwidth	56 GHz[1]
Phase noise	Less than -80 dBc/Hz @ 10 kHz
Reference oscillator	High precision TCXO, stability: 100 ppb
Antenna	34.4 dBi PTFE lens, HPBW: 2.7°

[1] Range resolution: 3.9 mm (3-dB bandwidth, Hann window).

the distance variation with respect to the actual radar-to-target distance.

For the sake of discussion, it is useful to define a metric, which rates the quality of far field

$$\alpha_{\mathrm{ff}} \stackrel{\mathrm{def}}{=} \frac{\lambda r}{D_1^2 + D_2^2}. \tag{20}$$

In accordance with the Fraunhofer distance, the value of α_{ff} increases with improved far-field conditions.

The transmitting aperture illumination functions at nine different frequencies were simulated on a plane 1 cm in front of the antenna. They were obtained by full-wave EM simulations using the time-domain solver in CST Microwave Studio. Fig. 3 exemplifies the results of the computed phase variations for the radar target with 5 cm of diameter. The set of curves represents the phase responses of systems describing the radar path's properties of free-space wave propagation for certain distances. It can be seen that these systems are a good approximation of generalized linear phase, i.e., linear phase with additional phase offset. For increasing and decreasing α_{ff}, the phase response tends to 0° and $-180°$, respectively.

The measured, the simulated, and the approximated distance variations for pulse position and pulse phase measurement are shown in Fig. 4(a) and (b). One can observe that the numerically simulated results match the real data quite well to within a few microns. As the assumptions made for the approximate closed-form expression, e.g., spherical wavefronts of constant amplitude, are satisfied in the far-field, the closed-form expression better approximates the real data as α_{ff} increases. Moreover, the pulse phase measurements are more closely approximated than the pulse position measurements. However, with increasing α_{ff}, the phase response becomes strictly linear (see Fig. 4); thus, the curves in Fig. 4(a) should approach with greater values of r, just like in Fig. 4(b).

By definition, the far-field region of the 5 cm radar target starts at 2.57 m. Nevertheless, at this distance, the actual deviation of reference points is still 80 to 90 μm, emphasizing the relevance of our investigations.

VI. CONCLUSION

We demonstrated the existence of distance variations due to near-field effects on free-space measurements with ultra-wideband mmWave radar. As these variations were up to a quarter wavelength, they were significant in micrometer accurate ranging applications. We propose two computational methods: a numerical simulation by means of physical optics (see Sections II and III) and an approximate closed-form expression (19). The theory was validated by sophisticated experiments, showing excellent agreement. Therefore, in practice, the proposed methods can be used to correct distance estimates without the need for time-consuming and expensive calibration in advance.

ACKNOWLEDGMENT

The authors would like to thank 2π-Labs GmbH for providing the radar sensor, and Status Pro Maschinenmesstechnik GmbH for straightening the linear guide.

REFERENCES

[1] Y. Y. Hu, "A method of determining phase centers and its application to electromagnetic horns," *J. Franklin Inst.*, vol. 271, no. 1, pp. 31–39, Jan. 1961.

[2] D. Waidelich, "The phase centers of aperture antennas," *IEEE Trans. Antennas Propag.*, vol. AP-28, no. 2, pp. 263–264, Mar. 1980.

[3] J. W. Odendaal and C. W. I. Pistorius, "A method to measure the aperture field and experimentally determine the near-field phase center of a horn antenna," *IEEE Trans. Instrum. Meas.*, vol. 42, no. 1, pp. 51–53, Feb. 1993.

[4] W. Kunysz, "Antenna phase center effects and measurements in GNSS ranging applications," in *Proc. IEEE Int. Symp. Antenna Technol. Appl. Electromagn. Amer. Electromagn. Conf.*, 2010, pp. 1–4.

[5] E. Nagelberg, "Fresnel region phase centers of circular aperture antennas," *IEEE Trans. Antennas Propag.*, vol. AP-13, no. 3, pp. 479–480, May 1965.

[6] M. R. Mahfouz, C. Zhang, B. C. Merkl, M. J. Kuhn, and A. E. Fathy, "Investigation of high-accuracy indoor 3-D positioning using UWB technology," *IEEE Trans. Microw. Theory Techn.*, vol. 56, no. 6, pp. 1316–1330, Jun. 2008.

[7] E. Muehldorf, "The phase center of horn antennas," *IEEE Trans. Antennas Propag.*, vol. AP-18, no. 6, pp. 753–760, Nov. 1970.

[8] R. Bhalla and H. Ling, "Three-dimensional scattering center extraction using the shooting and bouncing ray technique," *IEEE Trans. Antennas Propag.*, vol. 44, no. 11, pp. 1445–1453, Nov. 1996.

[9] Q. Li, E. J. Rothwell, K.-M. Chen, and D. P. Nyquist, "Scattering center analysis of radar targets using fitting scheme and genetic algorithm," *IEEE Trans. Antennas Propag.*, vol. 44, no. 2, pp. 198–207, Feb. 1996.

[10] M. Hurst and R. Mittra, "Scattering center analysis via Prony's method," *IEEE Trans. Antennas Propag.*, vol. AP-35, no. 8, pp. 986–988, Aug. 1987.

[11] L. Piotrowsky, T. Jaeschke, S. Kuppers, and N. Pohl, "An unambiguous phase-based algorithm for single-digit micron accuracy distance measurements using FMCW radar," in *Proc. IEEE MTT-S Int. Microw. Symp.*, 2019, pp. 552–555.

[12] L. Piotrowsky, T. Jaeschke, S. Kueppers, J. Siska, and N. Pohl, "Enabling high accuracy distance measurements with FMCW radar sensors," *IEEE Trans. Microw. Theory Techn.*, vol. 67, no. 12, pp. 5360–5371, Dec. 2019.

[13] L. Piotrowsky and N. Pohl, "Spatially resolved fast-time vibrometry using ultrawideband FMCW radar systems," *IEEE Trans. Microw. Theory Techn.*, vol. 69, no. 1, pp. 1082–1095, Jan. 2021.

[14] M. Pauli *et al.*, "Miniaturized millimeter-wave radar sensor for high-accuracy applications," *IEEE Trans. Microw. Theory Techn.*, vol. 65, no. 5, pp. 1707–1715, May 2017.

[15] S. Scherr *et al.*, "Influence of radar targets on the accuracy of FMCW radar distance measurements," *IEEE Trans. Microw. Theory Techn.*, vol. 65, no. 10, pp. 3640–3647, Oct. 2017.

[16] S. Scherr, S. Ayhan, B. Fischbach, A. Bhutani, M. Pauli, and T. Zwick, "An efficient frequency and phase estimation algorithm with CRB performance for FMCW radar applications," *IEEE Trans. Instrum. Meas.*, vol. 64, no. 7, pp. 1868–1875, Jul. 2015.

[17] N. Pohl *et al.*, "Radar measurements with micrometer accuracy and nanometer stability using an ultra-wideband 80 GHz radar system," in *Proc. IEEE Topical Conf. Wireless Sensors Sensor Netw.*, 2013, pp. 31–33.

[18] A. Stelzer, C. G. Diskus, K. Lubke, and H. W. Thim, "A microwave position sensor with submillimeter accuracy," *IEEE Trans. Microw. Theory Techn.*, vol. 47, no. 12, pp. 2621–2624, Dec. 1999.

[19] R. Stolle and B. Schiek, "Multiple-target frequency-modulated continuous-wave ranging by evaluation of the impulse response phase," *IEEE Trans. Instrum. Meas.*, vol. 46, no. 2, pp. 426–429, Apr. 1997.

[20] M. Scherhaufl, F. Hammer, M. Pichler-Scheder, C. Kastl, and A. Stelzer, "Radar distance measurement with Viterbi algorithm to resolve phase ambiguity," *IEEE Trans. Microw. Theory Techn.*, vol. 68, no. 9, pp. 3784–3793, Sep. 2020.

[21] A. Bhutani, S. Marahrens, M. Gehringer, B. Goettel, M. Pauli, and T. Zwick, "The role of millimeter-waves in the distance measurement accuracy of an FMCW radar sensor," *MDPI Sensors*, vol. 19, no. 18, Sep. 2019, Art. no. 3938.

[22] G. Vinci, S. Lindner, F. Barbon, R. Weigel, and A. Koelpin, "Promise of a better position," *IEEE Microw. Mag.*, vol. 13, no. 7, pp. S41–S49, Nov./Dec. 2012.

[23] F. Michler, B. Scheiner, T. Reissland, R. Weigel, and A. Koelpin, "Micrometer sensing with microwaves: Precise radar systems for innovative measurement applications," *IEEE J. Microw.*, vol. 1, no. 1, pp. 202–217, Jan. 2021.

[24] S. A. Schelkunoff, "Some equivalence theorems of electromagnetics and their application to radiation problems," *Bell Syst. Techn. J.*, vol. 15, no. 1, pp. 92–112, Jan. 1936.

[25] W. V. T. Rusch, A. C. Ludwig, and W. C. Wong, "Analytical techniques for quasi-optical antennas," in *Handbook of Antenna Design*, vol. 1. London, U.K.: Inst. Elect. Eng., 1982, pp. 60–127.

[26] D. M. Kerns and E. S. Dayhoff, "Theory of diffraction in microwave interferometry," *J. Res. Nat. Bur. Standards*, vol. 64B, no. 1, pp. 1–13, Jan. 1960.

[27] J. Ala-Laurinaho, Z. Du, V. Semkin, V. Viikari, and A. V. Raeisaenen, "Reflection coefficient method for antenna radiation pattern measurements," in *Proc. Eur. Radar Conf.*, 2015, pp. 285–288.

[28] M. A. Eberspacher, "Simulation method for multiple reflections in near-field applications," in *Proc. German Microw. Conf.*, 2019, pp. 202–205.

[29] B. Hattenhorst, L. Piotrowsky, N. Pohl, and T. Musch, "An mmWave sensor for real-time monitoring of gases based on real refractive index," *IEEE Trans. Microw. Theory Techn.*, vol. 69, no. 11, pp. 5033–5044, Nov. 2021.

[30] S. Kueppers, T. Jaeschke, N. Pohl, and J. Barowski, "Versatile 126182 GHz UWB D-band FMCW radar for industrial and scientific applications," *IEEE Sensors Lett.*, vol. 6, no. 1, Jan. 2022, Art. no. 3500204.